

# Optimized Design of Medium Frequency Transformers with High Isolation Requirements

G. Ortiz, J. Biela and J. W. Kolar  
 Power Electronic Systems Laboratory, ETH Zurich  
 ETL I16, Physikstrasse 3  
 CH-8092 Zurich, Switzerland  
 Email: ortiz@lem.ee.ethz.ch

**Abstract**—For future DC electric power systems, high-power DC-DC converters will play a major role as they will substitute today’s bulky 50/60Hz transformers. One key component within this DC-DC converters is the medium frequency transformer that provides the isolation level and the step up/down of the different voltage levels. As a consequence, an optimized design methodology that considers this high isolation requirements is needed. This paper presents a step-by-step design for medium frequency transformers with high isolation requirements. Each step in the design is carefully discussed and the required design considerations, such as flux density limits, isolation and thermal management, are explained in detail. The proposed design procedure is applied to a core-type transformer analyzing the outcome of the optimization process.

## I. INTRODUCTION

With increasing integration of renewable energy generation into power grids, distribution using DC level is becoming more and more attractive. For example, as wind farms are installed in the seas and far from the shore, DC transmission outcomes AC transmission in terms of efficiency because no reactive power is generated/consumed by the transmission cable. Furthermore, by replacing the bulky 50/60Hz transformers by higher-frequency transformers, a considerable reduction in weight/volume, hence installation costs, could be achieved. This new concept has been evaluated in [1] and [2], where high power DC-DC converters in the MW range are required to interface the different voltage levels within the wind farm.

On the other hand, energy generation with renewable energy sources is highly sensitive to variations in the natural conditions [3]. For instance, photovoltaic panels can only supply energy during daylight and therefore they must be paired with large-sized storage systems to supply the demanded energy in absence of enough sunlight. Here, the photovoltaic generators must be interfaced with their respective storage systems through a high-power bidirectional DC-DC converter which can dynamically control the power within the system and to the power grid.

As can be seen, high-power DC-DC converters are enabling technologies for this future power generation scene [4]. A schematic representation of a high-power DC-DC converter interfacing two voltage levels, i.e. Low-Voltage (LV) and High-Voltage (HV), is shown in Fig. 1. The task of the MF transformer is essentially the same as with 50/60Hz transformers: provide step-up/down in voltage levels and insure electrical isolation between LV and HV sides, which must comply with international standards [5]. In this MF transformer, the excitation frequency provided by

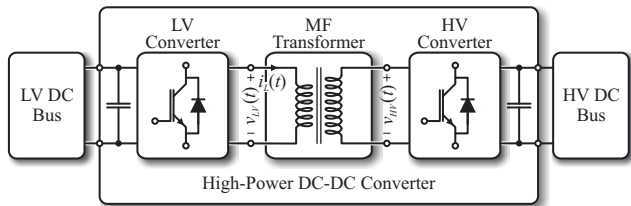


Figure 1: DC-DC converter interfacing two DC grids with different voltage levels.

TABLE I: Specifications for the isolated, bidirectional DC-DC converter: Step 1.

| Parameter                                   | Value       |
|---|-------------|
| Power $P$                                   | 1 MW        |
| Switching frequency $f_s=1/T_s$             | 20 kHz      |
| Port 1 voltage (High Voltage side) $V_{HV}$ | 12 kV       |
| Port 2 voltage (Low Voltage side) $V_{LV}$  | 1.2 kV      |
| Isolation $V_{ins}$                         | 100 kVDC    |
| Turns ratio $n$                             | 12          |
| Leakage Inductance $L_\sigma$               | 1.6 $\mu$ H |

the power electronic components is several times higher as in traditional 50/60 Hz systems, leading to a significant reduction in the transformer’s overall size and weight. In Fig. 2, a map with transformer design from different research groups with their operating frequencies and achieved volumes is shown. Here with increased operating frequencies, a great volume reduction can be noticed where the break in the fitted line is given by a change in the utilized core material.

However, with higher frequencies, effects such as skin and proximity, hysteresis losses and dielectric losses are significantly increased in relation to operation at 50/60Hz. Moreover, the reduction in size usually implies an increased loss density in the transformer, which demands considerable thermal management efforts [6]. It is therefore required to develop a clear design procedure for MF transformers that accounts for High-Frequency (HF) effects, isolation requirements and thermal management of the transformer among others.

Previous research efforts devoted to the design of MF transformers for traction applications are [7–9]. More recently, in [6] and [10], the design considerations for MF transformers in renewable energy applications was studied. However, an optimized design procedure which can clearly state the optimization limits of the MF transformer for given set of selected materials is not yet studied.

This paper presents a step-by-step design of single-phase MF transformers which enables the identification of the optimum design parameters for a given optimization figure. Special attention is

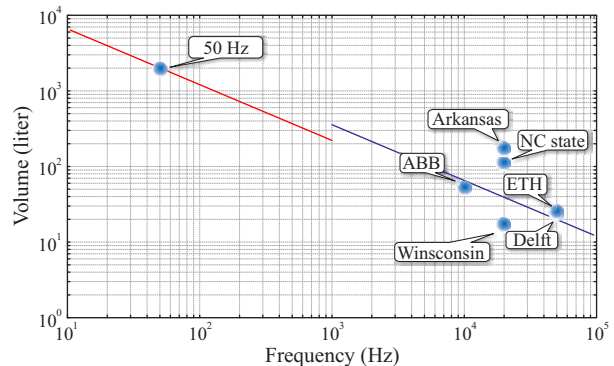


Figure 2: Volume reached by different transformer designs with different operating frequencies (all scaled to 1 MW power rating).

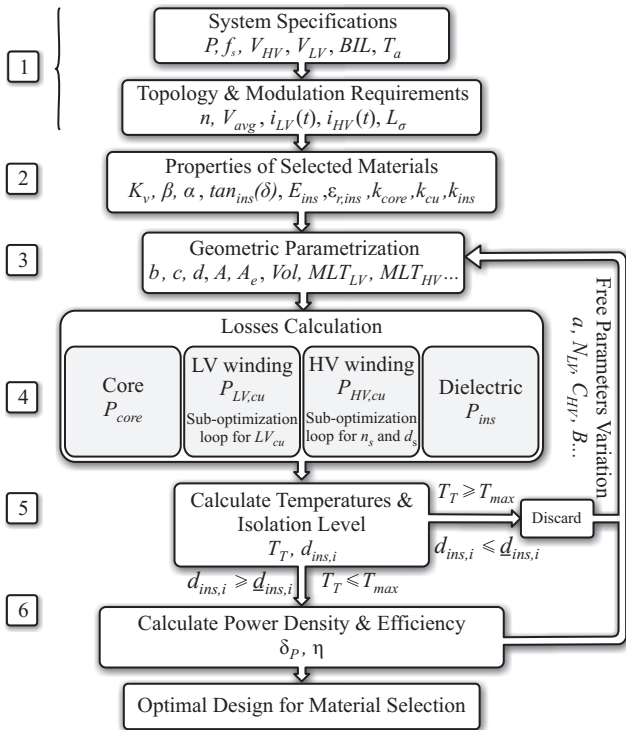


Figure 3: Design flow-chart of the MF transformer.

paid to the effect of the isolation requirement on efficiency, power density and heat extraction efforts. In **Section II**, the design flowchart of the transformer is presented and each step in the design flow is discussed in detail. As the MF transformer has a significant impact on the converter's efficiency, power density and mechanical arrangement, a design example using the specifications of Table I is given in **Section III**, following the proposed methodology.

## II. MEDIUM-FREQUENCY TRANSFORMER DESIGN

The proposed design flow for the MF transformer is shown in Fig. 3. A summary of this design procedure is described as follows.

- 1) Previous to the optimization, the requirements from a system point of view are introduced into a circuit calculator which outputs the waveforms, turns ratio and required leakage inductance of the transformer.
- 2) Conductor, isolation and core material properties are introduced.
- 3) The geometry of the transformer parts are then parameterized with respect to free variables, which are varied during the design process in order to reach an optimum design.
- 4) With the geometric design parameters, the losses in the core, windings and insulation medium are calculated considering HF effects.
- 5) Using thermal models, the temperatures of the components are estimated and the reached isolation level is calculated. If both parameters fulfil the requirements, the results are stored and another set of parameters is selected to perform the next design process.
- 6) Once all combinations of free parameters have been tested, the optimal set of free parameters for a given optimization criteria (i.e. efficiency or power density) can be extracted. A new optimization process can be started with a different selection of materials to perform a comparison of the trade-offs between these materials.

The means to perform each of these design steps are now detailed.

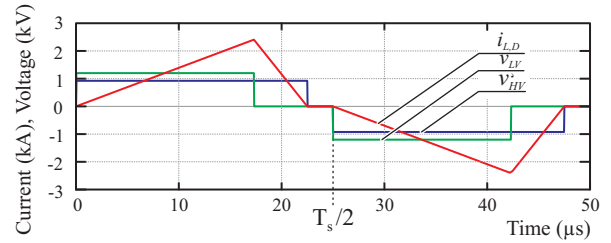


Figure 4: Voltage and current waveforms for DAB converter with triangular modulation designed for specifications of Table I.

### A. System Specifications and Modulation Requirements: Step 1

The system specifications (cf. Table I) are introduced into a circuit calculator including the topology and modulation of the converter. This circuit calculator outputs the applied input and output voltage waveforms  $v_{LV}(t)$ ,  $v_{HV}(t)$  and the current  $i_L(t)$  as defined in Fig. 1. These waveforms will thereafter determine the required HV and LV windings turns, the core cross section and the characteristics of the copper conductors, among others. As an example, the voltage and current waveforms considering a Dual Active Bridge (DAB) with triangular modulation [11] are shown in Fig. 4.

As can be seen, the voltages applied to the transformer are square-shaped, which is the most common case for DC-DC converters. However, as explained in the next section, arbitrary voltage waveforms can be considered as only the average applied voltage over one half period is required in the design process. On the other hand, the current waveform determines the thickness or diameter of the copper conductors, which in general case can be optimized for arbitrary current waveforms [12].

### B. Material Selection: Step 2

1) *Core Material*: The characteristics, namely the saturation flux and the losses, of the core material have a great impact on the power density and efficiency of the transformer, as they fix the maximum operating flux density. In 50/60Hz line transformers, typical used core materials are silicon-steel, nickel-steel and nanocrystalline. At higher excitation frequencies, other core materials are more attractive due to their lower specific losses. A list of most commonly used core materials in higher-frequency applications is presented in Table. II.

As can be seen, the selected materials present high saturation fluxes and low specific losses, specially in the case of amorphous and nanocrystalline materials with saturation fluxes in the 1.2 to 1.6T range and specific losses (at  $B=1$  T and  $f_s=20$  kHz) in the range of 0.04 kW/kg to 1.5 kW/kg. However, these materials have usually a considerable higher cost because of their manufacturing processes. The saturation flux and specific losses are defining the flux density limit, and thus this topic is now addressed.

Consider a periodic voltage applied to a coil with effective cross section  $A_e$  and number of turns  $N_{LV}$ . The maximum flux density

TABLE II: Core materials considered in high-power MF transformers. Up: Amorphous, Middle: Nanocrystalline, Down: Silicon Steel.

| Series               | Sat. Flux | Sp. losses | Manufacturer  |
|----------------------|-----------|------------|---------------|
| Micro-lite (2605SA1) | 1.56 T    | 1.5 kW/kg  | Metglas [13]  |
| Powerlite (2605SA1)  | 1.56 T    | 0.6 kW/kg  | Metglas       |
| Namglass             | 1.59 T    | 0.34 kW/kg | Magmet [14]   |
| Vitrovac (6030F)     | 0.82 T    | 0.19 kW/kg | VAC [15]      |
| Finemet (FT-3M)      | 1.23 T    | 0.14 kW/kg | Hitachi [16]  |
| Vitroperm (500F)     | 1.2 T     | 0.07 kW/kg | VAC           |
| Nanoperm             | 1.2 T     | 0.04 kW/kg | Magmetec [17] |
| Namglass 4           | 1.23 T    | 0.04 kW/kg | Magmet        |
| Arnon 7 (3-6%Si,Fe)  | 1.53 T    | 1.6 kW/kg  | Arnold [18]   |
| Arnon 5 (3-6%Si,Fe)  | 1.48 T    | 1.06 kW/kg | Arnold        |

TABLE III: Typical dry-type insulation mediums and parameters (datasheet values).

| Isolation Type | Material     | Dielectric Strength | Loss Tangent        |
|----------------|--------------|---------------------|---------------------|
| Potted         | EPOXY        | 16 kV/mm            | 0.02 (@ 100 kHz)    |
| Potted         | Micares [19] | 8-24 kV/mm          | 0.01-0.08 (@ 50 Hz) |
| HV cable       | Silicone     | 4-28 kV/mm          | 0.005 (@ 1 GHz)     |
| HV cable       | PVC          | 9.8-19 kV/mm        | -                   |
| HV cable       | HDPE         | 19 kV/mm            | 0.0002 (@ 100 MHz)  |

in this coil is given by:

$$\hat{B} = \frac{1}{4N_{LV}A_e} V_{avg} T_s, \quad (1)$$

where  $V_{avg}$  corresponds to the average applied voltage over half a switching period  $T_s$ . Solving (1) for  $A_e$  gives the design equation for the required core effective cross section:

$$A_e = \frac{1}{4N_{LV}\hat{B}} V_{avg} T_s \quad (2)$$

The maximum operating flux  $\hat{B}$  is left as free design parameter with an upper boundary set by the saturation flux  $B_{sat}$  of the material. Usually, a 10% to 20% safety margin is introduced by transformer designers between  $\hat{B}$  and  $B_{sat}$  to avoid operation close to saturation due to possible small asymmetries in the applied voltage or transients. In this case, a flux balancing mechanism which actively controls the maximum flux density in the core would enable operation under safe conditions at all times with even smaller safety margins.

As shown later in Section II-D1, the power losses in the core material are increasing with increasing peak flux density  $\hat{B}$ , leading to an increased temperature rise in this component. It is therefore necessary to include a thermal model of the transformer (cf. Section II-E) to insure that the operating temperature is kept within safe values. If with the selected peak flux density the core temperature rises beyond these margins, the design is discarded and a new design process (cf. Fig. 3) is started with a new set of free parameters.

2) *Isolation and Leakage Inductance*: In literature, the core cross section times core window area product has been used as a figure to analyze the power density of the transformer. This figure is found to be inversely proportional to material properties as maximum current density of the conductors and peak operating flux density of the core [6]. However, to design a transformer using this parameter, its losses are required to be evaluated. Moreover, this figure does not contain the influence of isolation levels in the volume of the transformer. As this MF transformer is expected to replace the functionality of 50/60 Hz transformers, the provided isolation level must meet with stringent international standards and thus its influence on the power density must be included in the design of the transformer.

The required isolation level can be translated into a minimum distance  $\underline{d}_{ins,i}$  between the conductors to be isolated through:

$$\underline{d}_{ins,i} = \frac{V_{ins}}{\nu E_{ins}}, \quad (3)$$

where  $E_{ins}$  is the dielectric strength of the isolation material provided by the manufacturer and  $V_{ins}$  is the voltage required to be isolated. In (3),  $\nu$  is used as a safe margin parameter. Scarce guidelines can be found in literature to select this parameter. In addition, the electric field non-uniformities in the insulator due to edges and corners in the conductors must also be taken into account. This electric field is changing for different transformer constructions, making it considerably complex to establish clear rules for the selection of this safety margin. In this paper, similar values for  $\nu$  as could be found in HV cable manufacturers datasheets were used to prepare the design example from section III.

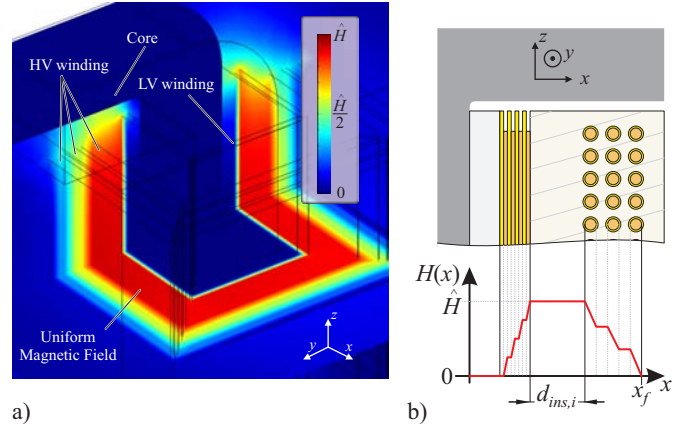


Figure 5: Magnetic leakage field distribution within transformer: a) 3D FEM magnetostatic simulation of a designed core-type transformer; b) Idealization of magnetic field distribution along the  $x$  axis.

The resulting distance  $d_{ins,i}$  (which is adjusted to reach the required leakage inductance  $L_{\sigma}$  as will be discussed later in this section) needs to be larger than minimum required distance  $\underline{d}_{ins,i}$  to fulfil the isolation requirements. If this requirement is not fulfilled, the design is discarded and a new design process is initiated with a new set of free parameters.

Different isolation materials have been used for transformers. Nowadays, dry-type isolation presents an attractive isolation solution for high power density systems. In this category, two isolation mechanisms can be found: Potted and HV cables. In potted isolation, the air from within the compounds must be extracted in a vacuum chamber to reduce the occurrence of partial discharges in the isolator. These systems usually operate under deep thermal cycles, leading to high thermomechanical stresses. These thermo-mechanical expansion could damage the isolation quality in the long term. To account for this problem, a soft potting material with a flexible mechanical characteristic is desirable.

HV cables on the other hand are built using a litz conductor merged into an insulator through high-pressure extrusion. By using a HV cable as insulation mechanism, the isolation complexity is considerably reduced as no custom made potting enclosures are required. However, with this construction the power density of the transformer is reduced because there is an unrequired double isolation layer between two adjacent HV turns.

A list of typical dry-type isolation materials and their properties is presented in Table III.

DC-DC converters usually require inductances in series with the transformer windings to achieve ZVS conditions. This inductance is defining the power transfer capability of the system and thus its value is carefully designed. In order to increase the power density of the converter, often this series inductance is magnetically integrated as leakage inductance  $L_{\sigma}$  of the transformer. This integration is translated into a constraint within the transformer design in which case a good estimation of the leakage inductance of the transformer is required.

In transformers with concentric windings, a good analytical estimation of the leakage inductance  $L_{\sigma}$  can be achieved as the magnetic field is mostly confined to the volume between the LV and HV windings. A magnetostatic FEM simulation of one design considering the described core-type transformer is shown in Fig. 5-a). Here it can be seen that the highest magnetic fields lie between the LV and HV windings and thus the magnetic field magnitude  $H$  can be ideally described by the graph presented Fig. 5-b). If homogeneous magnetic field distribution is considered along the  $y$  and the  $z$  axes, the stored magnetic energy within  $d_{ins,i}$  is

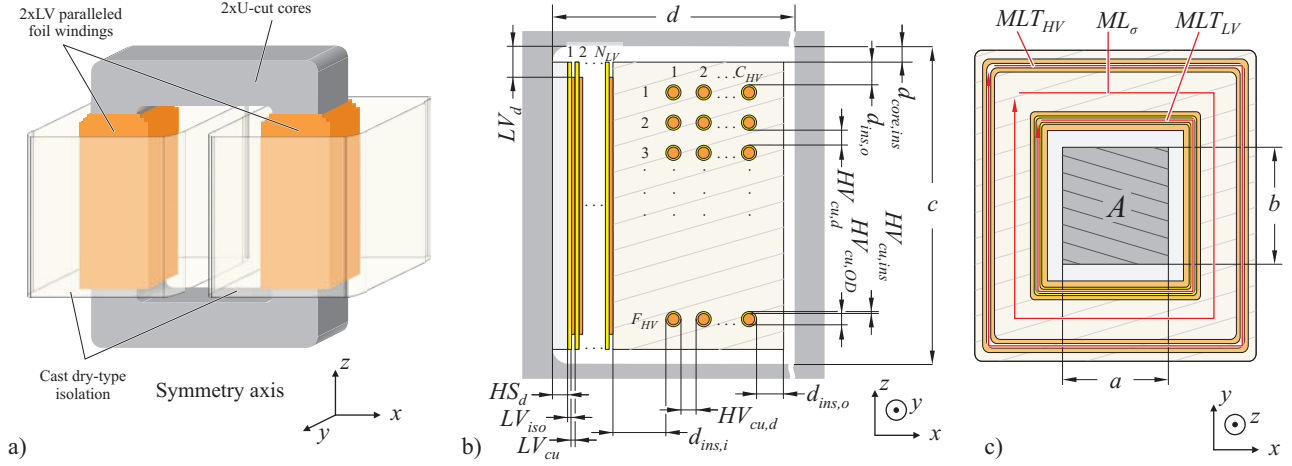


Figure 6: Core-type transformer used as reference: a) Winding arrangement; b) Winding window cross sectional view; c) Core cross-sectional view.

calculated from:

$$E_H = \frac{\mu_0 c M L_\sigma d_{ins,i}}{2} \cdot \hat{H}^2 = \frac{\mu_0 M L_\sigma d_{ins,i} N_{LV}^2 i_{LV}^2}{2c}, \quad (4)$$

where  $c$  is the core window height (cf. Fig. 6-b) and  $M L_\sigma$  corresponds to the mean length of the leakage path which can vary for different transformer concepts and winding arrangements. For the core-type transformer shown in Fig. 6-c) this length is:

$$\begin{aligned} M L_\sigma &= 8(N_{LV}(LV_{cu} + LV_{iso}) + HS_d) + 2(a + b + 2 \cdot d_{ins,i}) \\ &= K + 4 \cdot d_{ins,i} \end{aligned} \quad (5)$$

The energy stored in the leakage inductor  $L_\sigma$  referred to the LV side is calculated from:

$$E_L = \frac{i_{LV}^2 \cdot L_\sigma}{2} \quad (6)$$

Equating  $E_H = E_L$ , replacing  $M L_\sigma$  from (5), solving for  $d_{ins,i}$  and taking the positive solution yields:

$$d_{ins,i} = -\frac{K}{8} + \sqrt{K^2 + 16 \frac{L_\sigma c}{N_{LV}^2 \mu_0}}, \quad (7)$$

where  $K$  is a geometric constant defined in (5). This expression is an important design equation as it explicitly relates the required insulation distance  $d_{ins,i}$  and the leakage inductance  $L_\sigma$ , which are both design specifications. Also, this expression may vary for different transformer constructions and may in some cases not be possible to obtain analytically.

In the described design procedure, the distance  $d_{ins,i}$  is adjusted to reach the desired leakage inductance using (7). This value is then compared with the minimum insulation distance  $\underline{d}_{ins,i}$  defined by (3). If the distance is not enough, the design is discarded and a new process is initiated.

The next step in the design consists on defining the transformer geometry depending on the different fixed and free parameters and on the selected material constants.

### C. Geometry Parametrization: Step 3

The geometric variables of the transformer must be parameterized with respect to the constants given by the selected materials and also with respect to the free parameters. These geometric variables are mainly given by the transformer construction concept and therefore, in order to describe the design procedure, the core-type transformer depicted in Fig. 6 is used as example. Thereafter, the design can be extended to other types of transformers as the ones presented in [4], which posses their respective geometric definitions.

The core-type transformer consists of two C-cut cores arranged as in Fig. 6-a). In this case, each leg of the transformer comprises a LV foil winding with  $N_{LV}$  turns. These windings are then parallel connected. Two HV windings, built with litz conductors, are then wound around each leg of the core. The total turn number considering the series connection is  $N_{HV}$  where the turns ratio  $n$  relates the HV and LV turns through:

$$N_{HV} = n \cdot N_{LV} \quad (8)$$

In Fig. 6-b), the winding arrangement is shown. At the left-most side of the winding window, a water-cooled heat sink with thickness  $HS_d$  is considered to cool the core and LV winding. Around this heat sink, the primary foil winding with its respective isolation is wound, building up a total of  $N_{LV}$  isolation/copper-foil layers. To insure a desired isolation level between LV and HV windings, the HV winding is potted within a high-isolation compound, where a  $d_{ins,i}$  distance is placed between the last LV foil and the HV winding. The HV winding is built with a layered construction consisting of  $C_{HV}$  columns and  $F_{HV}$  rows. The distance from the HV winding to the outer face of the cast isolation is  $d_{ins,o}$ . With the definitions from Fig. 6-a), the following relation stands for the HV winding arrangement:

$$F_{HV} = \text{round}\left(\frac{n N_{LV}}{C_{HV}}\right) \quad (9)$$

The HV conductor has a  $HV_{cu,OD}$  diameter and its isolation thickness is defined as  $HV_{cu,ins}$ . The distance between adjacent HV turns is  $HV_{cu,d}$  and the distance from the cast isolation to the core is  $d_{core,ins}$ .

Using Fig. 6, the dimensions of the core winding window are given by:

$$\begin{aligned} c &= 2(d_{core,ins} + d_{ins,o}) + F_{HV}(HV_{cu,OD} + 2HV_{cu,ins}) \\ &\quad + (F_{HV} - 1)HV_{cu,d} \quad (10) \\ d &= 2(HS_d + N_{LV}(LV_{cu} + LV_{iso}) + d_{ins,i} \\ &\quad + C_{HV}(HV_{cu,OD} + 2HV_{cu,ins}) + (C_{HV} - 1)HV_{cu,d}) \quad (11) \end{aligned}$$

The geometric cross section  $A = a \cdot b$  of the core is shown in Fig. 6-c). By equating  $A_e = \kappa A$  and solving for  $b$  the following expression is found:

$$b = \frac{V_{avg}}{4f_s n N_{LV} \hat{B} \cdot \kappa \cdot a}, \quad (12)$$

where  $\kappa$  represents the stacking factor of the core.

It should be noted that nowadays magnetic cores for these type of applications are typically tailored for specific customer requirements. It is therefore possible select arbitrarily the dimensions  $a$ ,  $b$ ,  $c$  and  $d$  of the core that fulfil the optimum design criteria for the given transformer concept.

#### D. Losses Calculation: Step 4

With the geometry of each transformer part defined, it is now possible to calculate the losses generated by these components under the current and voltage excitations described in Section II-A. The losses sources in a transformer are mainly four: Core material, LV winding, HV winding and insulator. The means to calculate each of these losses are now detailed.

1) *Core Losses*: Considerable effort has been devoted to calculation of core losses under non-sinusoidal excitation [20–22]. Further methods and comparison of them was performed in [23]. In the present design procedure, the approach described in [20] is implemented and its application is straightforward since only the sinusoidal Steinmetz parameters along with the voltage waveforms are required for the computation.

2) *LV Copper Foil Losses*: The analytical calculation of the HF losses for a given sinusoidal AC current in a foil winding was done in [24] and applied to the LV winding of the core-type transformer described in Section II-C yields:

$$P_{f,n} = R_{DC,f} \frac{LV_{cu}}{\delta_{0,n}} \left[ \underbrace{F_{f,n} \cdot i_{LV,n}^2}_{Skin} + \underbrace{G_{f,n} \cdot \frac{2(N_{LV}^2 - 1)}{3} \cdot i_{LV,n}^2}_{Proximity} \right] \quad (13)$$

$$R_{DC,f} = N_{LV} \frac{\rho_{cu} MLT_{LV}}{LV_{cu} \cdot (c - 2LV_d)}, \quad (14)$$

where  $\rho_{cu}$  is the resistivity of copper,  $i_{LV,n}$  is the  $n$ -th harmonic component of the current,  $\delta_{0,n}$  is the skin depth,  $F_{f,n}$  is the skin effect factor for foils and  $G_{f,n}$  is the proximity effect factor for foils. The expressions for these last three parameters can be reviewed in [24]. The external magnetic field  $H_{e,f}$  depends on the winding arrangement and for the construction presented in Fig. 6 the expression given in (13) is valid. The mean length of the LV winding  $MLT_{LV}$  is calculated by using the definitions from Fig. 6-c):

$$MLT_{LV} = 4(N_{LV}(LV_{cu} + LV_{iso}) + 2HS_d) + 2(a + b) \quad (15)$$

The overall losses in the conductor can be calculated by adding the individual contributions of each current harmonic component:

$$P_{LV} = \sum_{n=1}^{\infty} P_{f,n} \quad (16)$$

In practice, (16) must be truncated by the designer when a defined precision in the loss calculation has been reached. Losses due to skin effect decrease by increasing the foil thickness whereas proximity effect losses increase with increasing foil thickness. As a consequence, an optimum value can be found, for example, implementing numerical solvers or using the approach presented in [12].

3) *HV Litz Copper Wire Losses*: The analytical calculation of the HF losses in a litz conductor is performed in [25]. Considering definitions of the core-type transformer given in Fig. 6, the power dissipated in one of the strands within the whole bundled litz conductor is calculated from:

$$P_{st,n} = R_{DC,st} \cdot \left[ \underbrace{F_{st,n} \cdot i_{HV,n}^2}_{Skin} + \underbrace{G_{st,n} \frac{i_{HV,n}^2}{8\pi^2 r_{bu}^2 \cdot n_s} + G_{st,n} \cdot F_{HV}^3 \frac{C_{HV}(4 \cdot C_{HV}^2 - 1)}{C^2} i_{HV,n}^2}_{Proximity} \right] \quad (17)$$

$$R_{DC,st} = N_{HV} \frac{4MLT_{HV} \rho_{cu}}{\pi d_s^2}, \quad (18)$$

where  $i_{HV,n}$  is the  $n$ -th harmonic of the HV side current,  $r_{bu}$  is the complete litz wire radius,  $d_s$  is the diameter of one strand and  $n_s$  is the total amount of strands in the conductor. The skin and proximity effect factors for a strand conductor are  $F_{st,n}$  and  $G_{st,n}$  respectively and their analytical expressions can be extracted from [24]. The mean length of one strand in the HV winding in the core-type transformer ( $MLT_{HV}$ ) is calculated following the definitions from Fig. 6-b) as:

$$MLT_{HV} = 2(4N_{LV}(LV_{cu} + LV_{iso}) + (HS_d + d_{ins,i})) + C_{HV}(HV_{cu,OD} + HV_{cu,ins}) + 2(C_{HV} - 1)HV_{cu,d} + (a + b). \quad (19)$$

In (17), three different sources for losses can be noticed: Skin effect, proximity due to the bundle internal magnetic fields, and proximity due to the external magnetic fields, i.e. other conductors in the winding arrangement. The external field  $H_{e,st}$  is given by the winding arrangement and for the concentric winding arrangement displayed in Fig. 6 the expression given in (17) is valid.

The total losses in the litz conductor are calculated from:

$$P_{HV} = n_s \cdot \sum_{n=1}^{\infty} P_{st,n} \quad (20)$$

This sum must be truncated once a defined precision in the loss calculation has been reached. An optimum value of strand diameter  $d_s$  and number of strands  $n_s$  can be found implementing numerical solvers.

4) *Dielectric Losses*: Dielectric losses in transformers are often low enough to be neglected in the design procedure. However, with increasing insulation requirements and operating frequencies, the losses in the dielectric material can reach considerable values.

Assuming a homogeneous electric field distribution within the insulator, the power dissipated in the Equivalent Series Resistor (ESR) of the insulator is calculated by:

$$P_{ins} = \frac{V_{ESR}^2}{ESR} = V_C^2 \cdot \tan(\delta) \cdot 2\pi f_s C_i, \quad (21)$$

where  $\tan(\delta)$  is often known as the dielectric loss factor and is defined by the insulation material,  $C_i$  is the capacitance between the isolated parts and  $V_C$  is the alternating voltage between the conductors. An accurate model of the capacitors present in a transformer and the analytical calculation of their capacitances was carried out in [26]. However, for a first approximation, the highest AC electric field can be assumed to be mostly confined to the space between the HV and LV windings, and thus, for the transformer presented in Fig. 6, a parallel plate approximation can be used to estimate this capacitance  $C_i$  and used to calculate the losses. It should be noted that the expression in (21) is thought for sinusoidal excitation thus errors are expected in its calculation.

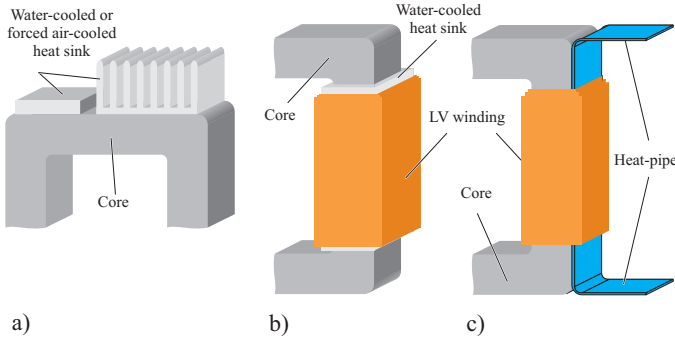


Figure 7: Core and LV winding cooling concepts: a) Water or forced-air cooled heat sink attached to top and bottom C-cut cores; b) Water cooled heat sink surrounding each leg of the core. c) Heat pipe surrounded by the LV winding.

### E. Thermal Management and Thermal Model: Step 5

The previously calculated power losses will generate heat, increasing the operating temperature of the transformer. To keep these temperatures within the allowed levels, it is necessary to use efficient cooling concepts. In order to achieve high power density in the transformer construction, active cooling concepts are preferred over passive heat extraction. Some of these active cooling concepts are now outlined for each of the parts generating losses within the transformer. The thermal model is then built using the selected thermal management concepts.

1) *Core*: Two heat extraction concepts for the core are presented in Fig. 7. In Fig. 7-a), the upper and lower surfaces of the core are used to extract the heat. The heat coming from the legs of the core are transported to these faces via thermal conduction through the core. The heat sinks used in this case may be forced air-cooled or water-cooled.

Another cooling mechanism that could be used in this case is a heat sink surrounding each leg of the core. With this mechanism, more surface of the core is in contact with the heat sink and therefore more heat could be extracted. It should be noted that by placing a water-cooled heat-sink surrounding the core, no significant losses are generated due to eddy currents because the magnetic field strength in this zone is relatively low (cf. Fig. 5-a)).

In laminated core materials as the ones presented in Table. II, the heat transfer is anisotropic as the thermal resistance can be considerably lower in the lamination direction as perpendicular to the lamination.

2) *LV Foil Winding*: The heat extraction mechanism presented in Fig. 7-b) can be easily extended to remove the heat from the LV winding. Here, the same water cooled heat sink is used to extract the LV winding heat and the core heat by winding the LV foil around this heat sink.

The LV winding can also be cooled by inserting a heat pipe between the inner turn and the core (cf. Fig. 7-c)). This heat pipe is then contacted with an external heat sink to remove the heat. This concept was studied in [27] where the temperature distribution along the heat pipe was analytically calculated.

3) *HV Litz Wire Winding and Insulator*: With high isolation requirements the HV winding presents increased heat extraction challenges as typically isolation materials possess low thermal conductivities. In case of a cast dry-type isolation, a heat extraction through the isolation material may be used. With this concept, the heat is conducted through the isolation material into externally attached heat sinks. These heat sinks may be water or air forced cooled. Special attention should be paid in this case to thermal cycles, as the isolation-heat sink contact may be deteriorated due to mechanical expansion caused by thermomechanical phenomena.

A second option for thermal extraction of the HV winding is to use a self-cooled wire comprising a braided copper litz conductor

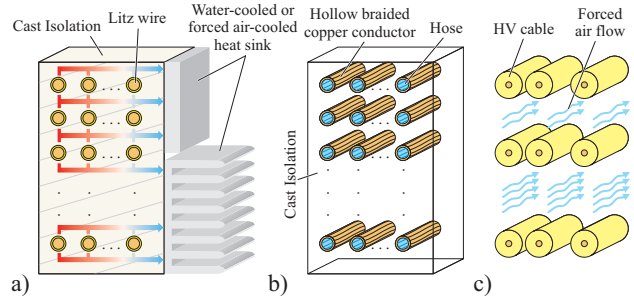


Figure 8: HV cooling concepts: a) Water or forced-air cooled heat sink attached to external face of cast insulation; b) Braided copper hollow conductor with internal plastic hose carrying water (self-cooled cable); c) Forced air cooled HV cable;

with a coaxial hose which carries water. This self-cooled wire is depicted in Fig. 8-b) and was proposed in [28] for a battery charging application.

In case a HV cable is used for the HV winding, limited options for heat extraction are possible since the copper conductor which generates the heat is merged within the isolator. In this case, forced air cooling through the cable presents an attractive solution. This concept is presented in Fig. 8-c).

It should be noted that the heat extraction of the HV winding is closely linked to the isolator heat extraction because this last component will always be tightly fixed with the HV conductor. For this reason, the heat extraction concepts described in this section are equally valid for the heat generated in the isolator.

To complete the transformer design, a thermal model of the arrangement is required in order to check if operating temperatures stay within the allowed values. The thermal models can vary significantly for different transformer concepts. In this case, the core-type transformer used as example throughout the paper is used to formulate the thermal model. The thermal management concepts employed in this case are the water-cooled heat sink for LV winding and core and an externally attached heat sink for the HV winding and isolation (i.e. Figs. 7-b) and 8-a) respectively). In this case, the main heat extraction mechanism is conduction with generation and therefore this mechanism is now studied.

Consider a solid heat conductor material as shown in Fig. 9 with width  $W$ , heat conduction  $k_M$ , homogeneous volumetric heat generation  $\dot{g}_M$  and whose temperature at its left hand side and right hand side is  $T_L$  and  $T_R$  respectively. An equivalent thermal circuit depicted in Fig. 9-b) can be formulated for the control section  $\Delta x$ . From this circuit the following equations are formulated for the temperature  $T_M(x)$  and the heat flux  $q_M(x)$ :

$$\frac{T_M(x)}{dx} = -k_M \cdot q_M(x) \quad (22)$$

$$\frac{q_M(x)}{dx} = \dot{g}_M \quad (23)$$

Combining (22) and (23) the differential equation for unidirectional steady-state heat conduction is found:

$$\frac{d^2 T}{dx^2} = -k_M \cdot \dot{g}_M \quad (24)$$

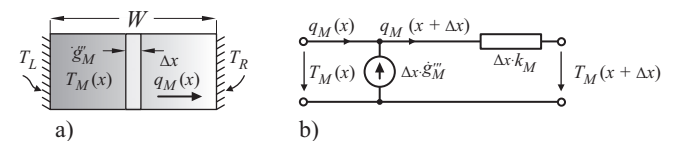


Figure 9: Heat conduction with volumetric heat generation: a) 1D heat conduction in a solid conductive material; b) Equivalent thermal-electric circuit for control section  $\Delta x$ .

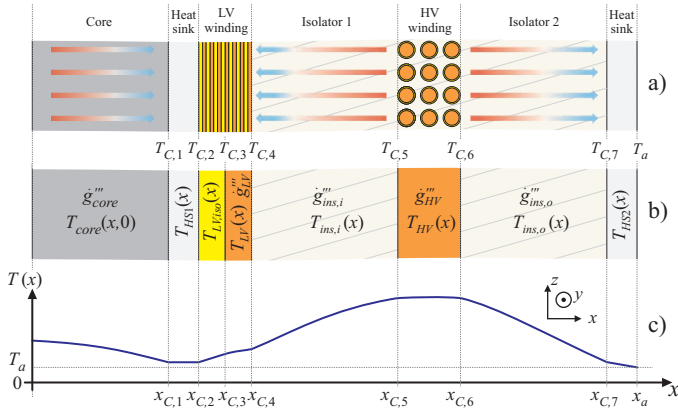


Figure 10: Core-type transformer heat model: a) Section used to build the heat model; b) Simplified geometry; c) Qualitative temperature profile in the transformer.

Integrating (24) twice and inserting the boundary conditions results in the solution for the temperature under unidirectional steady-state heat conduction with generation:

$$T_M(x) = -\frac{k_M \cdot \dot{g}_M'''}{2} x^2 + \left[ \frac{T_R - T_L}{W} + \frac{k_M \cdot \dot{g}_M'''}{2} W \right] x + T_L \quad (25)$$

The heat generation in the studied transformer takes place in the core, the LV winding, the isolation and in the HV winding. A section of the transformer design considering  $N_{LV}=7$  and  $C_{HV}=3$  is shown in Fig. 10-a) while a simplified version used to build the thermal model is presented in Fig. 10-b).

It should be noted that the portion of isolation between the HV winding and the outer heat sink is also generating losses since the heat sink must be grounded and therefore the isolator in this region also operates under high electric fields. The temperature distribution in the core was calculated using 2D heat conduction with generation and the equations can be revised in [29].

For each of the sections in Fig. 10-b) the expression in (25) is used to describe the temperature along the  $x$  axis where the left hand side and right and side temperatures  $T_L$  and  $T_R$  as well as the width  $W$  must be replaced accordingly extracting the geometric definitions from the previous design steps. The heat flux in the thermal interfaces must be equal for adjacent sections, for example, the heat flux on the right hand side of the LV winding must be equal to the heat flux on the left hand side of isolator 1, i.e.  $q_{LV}(x = x_{C,4}) = q_{ins,i}(x = x_{C,4})$ . By applying this constraint on each of the interfaces, a system of equations is found where the solutions are the interface temperatures  $T_{C,1}$  through  $T_{C,7}$ .

A qualitative thermal profile considering the presented thermal model is depicted in Fig. 10-c). The sections which possess volumetric heat generation show a parabolic temperature profile as described by (25). The highest temperature is expected in the HV winding given the typically low heat conduction of isolation materials.

### III. DESIGN EXAMPLE

To apply the procedure on a design example, the specifications from Table I are used together with the topology and waveforms described in Section II-A. From Fig. 6 it can be seen that a great number of geometric parameters must be defined to perform a design of the transformer. It is not practical to set all of these parameters as free, as the design procedure would become extremely cumbersome and long-lasting. It is the task of the designer to identify which of these parameters must be fixed given their influence in the transformer design. In this example, the free parameters are the core leg dimension  $a$ , the number of turns in the LV side  $N_{LV}$ , the rows in the HV winding  $C_{HV}$  and the maximum

TABLE IV: Fixed parameters for design example.

| Parameter                                       | Value  |
|---|--------|
| $HS_d$  | 5 mm   |
| $LV_{iso}$                                      | 0.1 mm |
| $HV_{cu,d}$                                     | 1 mm   |
| $HV_{cu,ins}$                                   | 0 mm   |
| $d_{core,ins}$                                  | 1 mm   |
| $\underline{d}_{ins,i} = \underline{d}_{ins,o}$ | 10 mm  |
| $\Delta T_{HV}$                                 | 60 °C  |
| $\nu$   | 41 %   |

flux density  $\hat{B}$ . Some of the fixed parameters are summarized in Table IV.

The core material selected is the nanocrystalline Vitroperm 500F whose saturation flux density  $B_{sat}$  is close to 1.1 T and therefore the absolute maximum operating flux density is set to  $\hat{B}=0.9$  T. However, smaller values are also used in the parametric sweep to study its influence on the optimization figures. The isolation material selected is the MICARES 720 [19], which has a dielectric strength  $E_{ins}$  of 24 kV/mm and the safety margin  $\nu$  is set to 41 %, thus the minimum isolation distance  $\underline{d}_{ins,i}$  as well as  $\underline{d}_{ins,o}$  are set to 10 mm. The maximum allowed temperature rise for the HV winding is 60 °C.

The design optimization in this case consists of a free parameter sweep where the maximums, minimums and step values can be seen in Fig. 11. The result of the parametric sweep can be seen in the efficiency - power density pareto front displayed in Fig. 12. Each dot represents a design of the transformer and its color shows the achieved HV winding peak temperature. The maximum achievable power density is 146 kW/liter with an efficiency of 99.75 % whereas the maximum reachable efficiency 99.79 % with a power density of 78 kW/liter. It is worth to note that the temperature of the HV winding is increasing directly with increasing power density.

In Fig. 12 the pareto fronts of the same transformer concept but considering a different core material (Vitrovac 6030F, cf Table II) and higher isolation requirement (150 kVDC) are also plotted. This additional pareto fronts show clearly the trade-offs that exist in the selection of different materials and specifications in the transformer design. The Vitrovac material features a lower saturation flux density and also higher specific losses and consequently lower efficiencies and power densities are achieved with this material. On the other hand, higher isolation requirements are translated into larger distances within the transformer and, as a consequence, the maximum achievable power density is reduced.

Fig. 11 shows the dependence of the optimization figures, i.e. power density and efficiency, for each of the free parameters. The power density and efficiency opti-

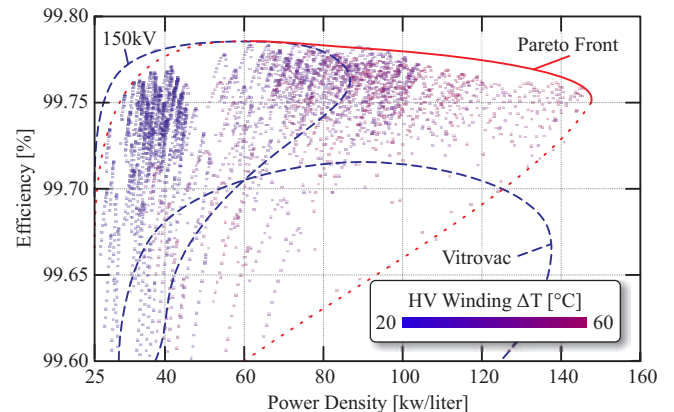


Figure 12: Transformer power density - efficiency pareto front for the optimized design of the core-type transformer.

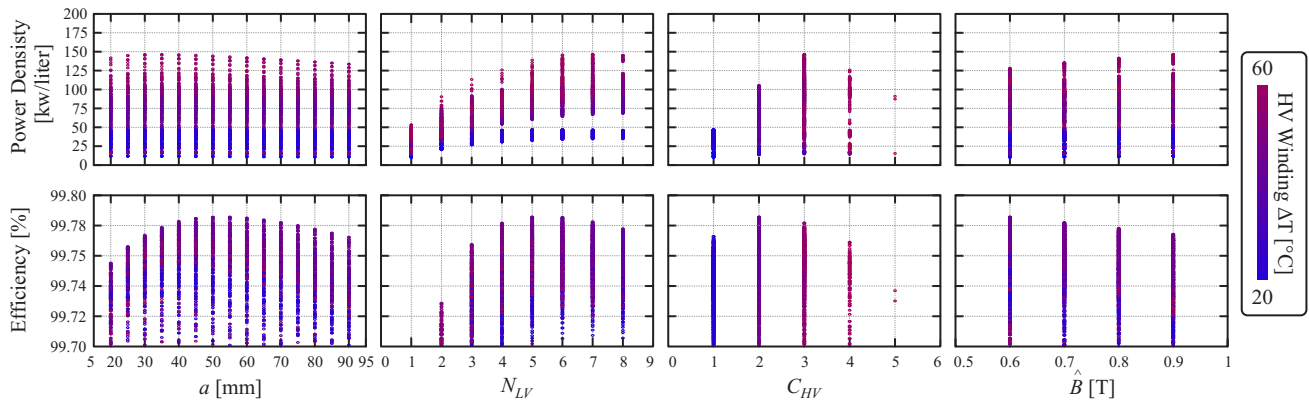


Figure 11: Power density and efficiency in dependence of the different free parameters.

mums are found at  $[a, N_{LV}, C_{HV}, \hat{B}] = [30 \text{ mm}, 7, 3, 0.9 \text{ T}]$  and  $[a, N_{LV}, C_{HV}, \hat{B}] = [55 \text{ mm}, 5, 2, 0.6 \text{ T}]$  respectively. From these graphs, also a sensitivity analysis can be performed. For example, the geometric parameter  $a$  is found to have much less influence in the power density as the HV winding columns  $C_{HV}$ . In case of the efficiency, its sensitivity is found to be larger with respect to the LV turns  $N_{LV}$  than to the peak flux density  $\hat{B}$ .

#### IV. CONCLUSIONS

A design methodology for MF transformers used in high-power DC-DC converters is presented. As this transformers must be a real replacement for today's 50/60Hz transformers, the design procedure gives special attention to the isolation reached by this transformer and its influence over other design parameters. This isolation requirement has an important impact over the design construction complexity of the system and also over its power density.

The design procedure was applied on a core-type transformer where the optimization figures were power density and efficiency. In the associated pareto fronts, the trade-offs between these two optimization figures were identified as well as the influence of different material selection and specifications. With the presented design procedure, the optimum free parameters are identified and the sensitivity of these parameters with respect to the optimization figures is easily analyzed.

#### V. ACKNOWLEDGEMENTS

The authors would like to acknowledge the European Center for Power Electronics - ECPE - for providing the financing of the research project.

#### REFERENCES

- [1] C. Meyer, "Key Components for Future Offshore DC Grids," Ph.D. dissertation, RWTH Aachen, 2007.
- [2] S. Lundberg, "Wind Farm Configuration and Energy Efficiency Studies - Series DC versus AC Layouts," Ph.D. dissertation, Department of Energy and Environment - Chalmers University of Technology, 2006.
- [3] P. Pinson, G. Papaefthymiou, B. Klockl, and J. Verboomen, "Dynamic sizing of energy storage for hedging wind power forecast uncertainty," in *Power Energy Society General Meeting*, July 2009, pp. 1–8.
- [4] G. Ortiz, J. Biela, D. Bortis, and J. W. Kolar, "1 megawatt, 20 khz, isolated, bidirectional 12kv to 1.2kv DC-DC converter for renewable energy applications," June 2010, pp. 3212–3219.
- [5] *IEEE Standard General Requirements for Dry-Type Distribution and Power Transformers Including Those With Solid Cast and/or Resin-Encapsulated Windings*, IEEE Std.
- [6] S. Meier, T. Kjellqvist, S. Norrga, and H.-P. Nee, "Design considerations for medium-frequency power transformers in offshore wind farms," in *Power Electronics and Applications EPE*, September 2009, pp. 1–12.
- [7] M. Steiner and H. Reinold, "Medium frequency topology in railway applications," September 2007, pp. 1–10.
- [8] T. Kjellqvist, S. Norrga, and S. Ostlund, "Design considerations for a medium frequency transformer in a line side power conversion system," vol. 1, June 2004, pp. 704–710.

- [9] H. Reinold and M. Steiner, "Characterization of semiconductor losses in series resonant dc-dc converters for high power applications using transformer with low leakage inductance," September 1999, pp. 1–10.
- [10] I. Villar, "Multiphysical Characterization of Medium-Frequency Power Electronic Transformers," Ph.D. dissertation, EPFL, April 9 2010.
- [11] F. Krismer, J. Biela, and J. Kolar, "A comparative evaluation of isolated bi-directional DC/DC converters with wide input and output voltage range," in *Industry Applications Conference*, vol. 1, October 2005, pp. 599–606 Vol. 1.
- [12] W. Hurley, E. Gath, and J. Breslin, "Optimizing the AC resistance of multilayer transformer windings with arbitrary current waveforms," *IEEE Transactions on Power Electronics*, vol. 15, no. 2, pp. 369–376, March 2000.
- [13] [Online]. Available: <http://metglas.com>
- [14] [Online]. Available: <http://www.magmet.com>
- [15] [Online]. Available: <http://www.vacuumschmelze.de>
- [16] [Online]. Available: <http://www.hitachi-metals.co.jp>
- [17] [Online]. Available: <http://www.magnetec.de>
- [18] [Online]. Available: <http://www.arnoldmagnetics.com>
- [19] [Online]. Available: [www.abb.com](http://www.abb.com)
- [20] K. Venkatachalam, C. Sullivan, T. Abdallah, and H. Tacca, "Accurate prediction of ferrite core loss with nonsinusoidal waveforms using only steinmetz parameters," in *Computers in Power Electronics*, June 2002, pp. 36–41.
- [21] J. Reinert, A. Brockmeyer, and R. De Doncker, "Calculation of losses in ferro- and ferrimagnetic materials based on the modified steinmetz equation," *Industry Applications, IEEE Transactions on*, vol. 37, no. 4, pp. 1055–1061, July 2001.
- [22] D. Lin, P. Zhou, W. Fu, Z. Badics, and Z. Cendes, "A dynamic core loss model for soft ferromagnetic and power ferrite materials in transient finite element analysis," *Magnetics, IEEE Transactions on*, vol. 40, no. 2, pp. 1318–1321, March 2004.
- [23] I. Villar, U. Viscarret, I. Etxeberria-Otadui, and A. Rufer, "Global loss evaluation methods for nonsinusoidally fed medium-frequency power transformers," *Industrial Electronics, IEEE Transactions on*, vol. 56, no. 10, pp. 4132–4140, October 2009.
- [24] P. Dowell, "Effects of eddy currents in transformer windings," *Electrical Engineers*, vol. 113, no. 8, pp. 1387–1394, August 1966.
- [25] J. A. Ferreira, "Analytical computation of AC resistance of round and rectangular litz wire windings," *IEE Proceedings B Electric Power Applications*, vol. 139, no. 1, pp. 21–25, 1992.
- [26] J. Biela, D. Bortis, and J. W. Kolar, "Analytical modeling of pulse transformers for power modulators," in *Power Modulator Symposium*, 2006, pp. 135–140.
- [27] J. Biela, D. Bortis, and J. Kolar, "Modeling of pulse transformers with parallel- and non-parallel-plate windings for power modulators," vol. 14, no. 4, August 2007, pp. 1016–1024.
- [28] C. Conrady, "High Power, High Frequency, Liquid-Cooled Transmission Cable and Charging Systems," U.S. Patent 5670 860, 1995.
- [29] G. Nellis, *Heat Transfer*, 1st ed. New York: Cambridge University Press, 2009.